

Phase Extraction from Interferogram using Machine Learning

Daichi Kando ^{*a} and Satoshi Tomioka ^b

^aGraduated School of Engineering, Hokkaido University, North-12 West-8, Kita-ku, Sapporo, Japan

^bFaculty of Engineering, Hokkaido University, North-12 West-8, Kita-ku, Sapporo, Japan

Abstract

Interferometric tomography can reconstruct 3D refractive index distributions through phase-shift measurements for different beam angles. To reconstruct a complex refractive index distribution, many projections along different directions are required. For the purpose of increasing the number of the projections, we earlier proposed a beam-angle-controllable interferometer with mechanical stages; however, the quality of some of extracted phase images from interferograms included large errors, because the background fringes cannot be precisely controlled. In this study we propose to apply machine learning to phase extraction, which has been generally performed by a sequence of several rule-based algorithms. In order to estimate a phase-shift image, we employ supervised learning in which input is an interferogram and output is the phase-shift image, and both are simulation data. As a result, the network after training can estimate phase-shift images almost correctly from interferograms, in which was difficult for the rule-based algorithms.

Background

Since the refractive index of an object or medium depends on its molecular density and number of electrons in a molecule, 3D distribution of gas temperature, electron density of the plasma, or concentration of a solute can be measured through a 3D measurement of refractive index of the medium. Computed tomography is well-known to reconstruct 3D internal distribution from line-integrated images with different integration paths. The line-integrated images of 3D refractive index distribution, which are 2D phase-shift images, are observed by using an interferometer. Therefore, the coupling of an interferometer and a technique of the computed tomography can realize a determination of the non-destructive 3D distribution of above-mentioned quantities such as gas temperature.

System

We have developed a 3D refractive index measurement system which consists of an incident-angle-controllable interferometer and data processing codes[1]. The figure 1 shows an experimental setup, which consists of two Mach-Zehnder interferometers. One of them has rotatable mirrors on movable stages, which are controllable and moving during acquisitions of interferograms for all angles.

A phase-shift image $\phi(\mathbf{r})$ is expressed as line integral of refractive index

$$\phi(\mathbf{r}) = \int_l (N(\mathbf{r}') - 1)k_0 dl(\mathbf{r}'), \quad (1)$$

and it is included in a observed interferogram $i(\mathbf{r})$ as

$$i(\mathbf{r}) = i_0(\mathbf{r})(1 + \cos(\phi(\mathbf{r}) + \delta\mathbf{k} \cdot \mathbf{r})), \quad (2)$$

where \mathbf{r} denotes the observation point on screen, l denotes the optical path, \mathbf{r}' denotes the field point in medium, $N(\mathbf{r}')$ denotes the refractive index distribution of the measurement medium, k_0 denotes the frequency of free space, $i_0(\mathbf{r})$ denotes the spatial mode of the light source, and $\delta\mathbf{k}$ denotes the spatial carrier frequency of the background fringe.

In general, to obtain the phase-shift images, we apply several processes to the acquired interferograms; an estimation of the spatial carrier frequency of the background fringe, a filtering in a spectral domain, a carrier frequency shifting, and a phase-unwrapping, which are rule-based algorithms. Figure 2 shows an example of phase extraction. The 3D refractive index distribution can be finally obtained by using computed tomography for the extracted phase-shift images.

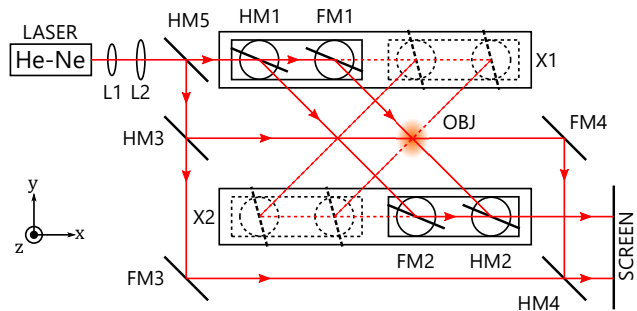


Figure 1. Incident-angle-controllable interferometer. The FM_n and the HM_n mean full- and half-mirrors, respectively. The beam is expanded to 50 mm diameter by two lenses of L1 and the L2. The OBJ means the object. The $HM1$, $FM1$, $FM2$, and $HM2$ are rotatable, and on the movable stages, X1 and X2.



Figure 2. An example of interferograms measured by an actual experiment and the extracted phase-shift images from the interferograms. This extraction is performed by rule-based algorithms.

Problem

This measurement system has two drawbacks. The first problem is limitation of exposure time. In this system, interferograms are acquired while the mirrors are moving. Therefore if the exposure time of the camera sets long, the interferograms are blurry by the mechanical vibration of the optical components. To reduce blurring of the interferograms the exposure time of the

camera to obtain the interferograms should be shortened, and the gain of the camera should be increased. As the result, the signal-noise ratios of the acquired interferograms become smaller. The second problem is uncontrollable background fringe patterns. In usual interferometric measurements, first, the interferogram both with and without the object are acquired. Next, the background fringe is removed from the former based on their difference. However, since the precision of the mechanical stage is several 10 microns whereas the wavelength of laser is about 0.6 microns, the background fringe patterns defined by a spatial carrier frequency vectors, which are different for the interferogram images of each incident beam direction, are not controllable and not repeatable.

To extract phase-shift image from interferogram successfully, an interval of background fringe must be in a certain range, and less noise of interferogram is preferred. However, from the above-mentioned restriction of the developed interferometer, these conditions are not always satisfied at any time. If these are not satisfied, the errors of the extracted phase-shift image are accumulated at each image process, or the phase extraction is failed. It causes the decrease of the number of available phase-shift images for reconstruction and affects the quality of the final 3D reconstructed distribution of the refractive index. To reduce the final error, we need to develop more accurate phase extraction algorithms for interferograms with many noises or under the unfavorable conditions.

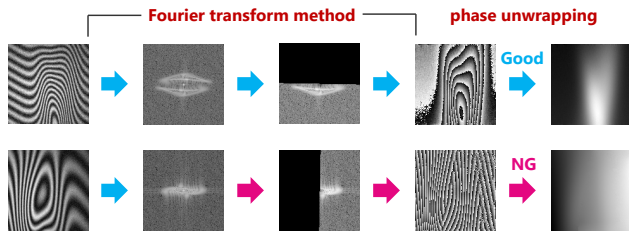


Figure 3. Examples of phase extraction using the rule-based algorithms. From left to right, the first arrows denote discrete Fourier transform, the second arrows denote removal of spatial mode of light source and complex conjugate component in Fourier space, the third arrows denote inverse discrete Fourier transform and carrier shift, and the last arrows denote phase unwrapping. These interferograms are simulated data. The top line and the bottom line show an example of successful and failed extraction, respectively.

Proposed method

In the last decade, machine learning has been applied in many fields including image processing. However, there are no studies for applications of phase extraction. In this study, we proposed a method which could directly extract phase-shift image from interferogram using machine learning, in which the processes such as phase-unwrapping were not required.

To estimate phase-shift image, we employed supervised learning in which input was interferogram and output was the corresponding phase-shift image. Since the phenomenon of interference is modeled as equation(2), we can readily generate interferogram through simulation under various given conditions such as phase-shift image, background fringe pattern and noise property.

We assumed phase-shift image using the following equation;

$$\phi(\mathbf{r}) = \sum_{j=1}^4 \phi_j G(\mathbf{r}; \mathbf{r}_{\phi_j}, \theta_{\phi_j}, a_{\phi_j}, b_{\phi_j}), \quad (3)$$

and the corresponding interferogram is expressed as this equation;

$$i(\mathbf{r}) = i_0(\mathbf{r})(1 + \cos(\phi(\mathbf{r}) + \delta \mathbf{k} \cdot \mathbf{r})) + i_{\text{noise}}(\mathbf{r}), \quad (4)$$

where

$$i_0(\mathbf{r}) = G(\mathbf{r}; \mathbf{r}_{i_0}, 0, a_{i_0}, b_{i_0}),$$

$$G(\mathbf{r}; \mathbf{r}', \theta, a, b) = e^{-(\mathbf{r}-\mathbf{r}') \cdot \mathbf{R}(\theta) \cdot \mathbf{W}(a,b) \cdot (\mathbf{r}-\mathbf{r}')},$$

$$\mathbf{R}(\theta) = \begin{pmatrix} \cos \theta & -\sin \theta \\ \sin \theta & \cos \theta \end{pmatrix},$$

$$\mathbf{W}(a, b) = \begin{pmatrix} a & 0 \\ 0 & b \end{pmatrix},$$

$$i_{\text{noise}}(\mathbf{r}) \sim N[0, \sigma_n] (\text{White, Normal}).$$

We provided ϕ_j , \mathbf{r}_{ϕ_j} , θ_{ϕ_j} , a_{ϕ_j} , b_{ϕ_j} , $\delta \mathbf{k}$, \mathbf{r}_{i_0} , a_{i_0} , b_{i_0} , and σ_n as random parameters. Ground truth is phase-shift image itself which is used when input data is generated. Totally 90,000 pairs of data were used; 80,000 pairs for training, and 10,000 pairs for test.

We use U-net[2] as the network architecture. The U-net has especially shown successful results in various image processing fields, and both input and output are images, therefore it is suitable for our study. To train the network, we employed Adam[3] implementation in Chainer[4], which is one of the frameworks for deep learning, as optimizer. The loss function during the training step was defined by the average of root mean squared error of the estimated output image from the ground truth

$$E_1 = \left\langle \sqrt{\left\langle (\phi_m(\mathbf{r}) - \phi(\mathbf{r}))^2 \right\rangle_{\text{pix}}} \right\rangle_{\text{image}}, \quad (5)$$

whereas the network during and after training was evaluated by the average of relative root mean squared error

$$E_2 = \left\langle \sqrt{\frac{\left\langle (\phi_m(\mathbf{r}) - \phi(\mathbf{r}))^2 \right\rangle_{\text{pix}}}{\left\langle (\phi(\mathbf{r}))^2 \right\rangle_{\text{pix}}}} \right\rangle_{\text{image}}, \quad (6)$$

where $\phi_m(\mathbf{r})$ denotes output phase-shift image from the network, and $\phi(\mathbf{r})$ denotes ground truth of phase-shift image. The training means iteration of updating the network parameters so that the value of the loss function E_1 becomes smaller.

Results

The figure 4 shows the evolution of the evaluation function. The vertical axis shows the evaluation function E_2 and the horizontal axis shows the epoch number. One epoch means that all training data was used once for training. The broken line shows the training data, and the solid line shows the test data. This graph shows that the training was successful, because the evaluation function for both the training data and the test data had been decreasing while the training.

Results for simulation data

The figure 5 shows examples of the results of the phase extraction from the simulated interferograms. From left to right, each image shows examples of the simulated interferograms as the test data, the ground truths of phase-shift images, the results of the phase extraction using the trained network, and the results of the phase extraction using the rule-based algorithms.

The figure 6 shows the histogram that the horizontal axis shows the value of evaluation function and the vertical axis shows the frequency of the data with the values on the horizontal axis. The 1754 of the extracted phases using the rule-based algorithms had the relative root mean squared error of more than 1.0, therefore they were excluded from the histogram and the average calculation.

The average of the relative root mean squared error of the test data between the ground truths and the extracted phases using the trained network is 0.025, meanwhile between the ground truths and the extracted phases using the rule-based algorithms is 0.461.

These results show that the phase extraction from the simulated interferograms using machine learning was successful and better than the rule-based algorithms.

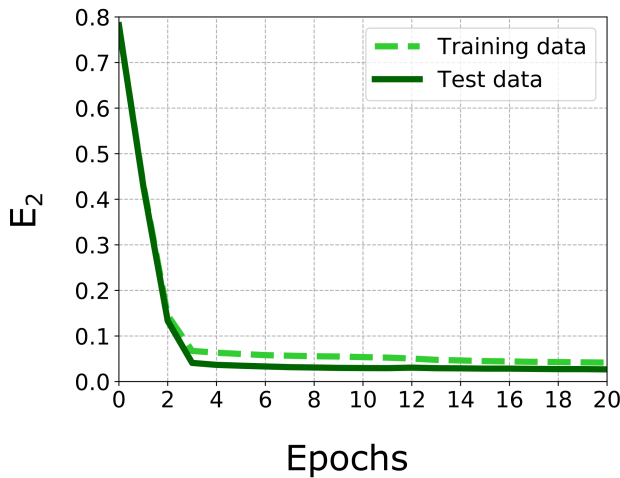


Figure 4. Evolution of the evaluation function E_2 . As the training progresses, E_2 of both the training data and the test data is decreasing. This training is successful.

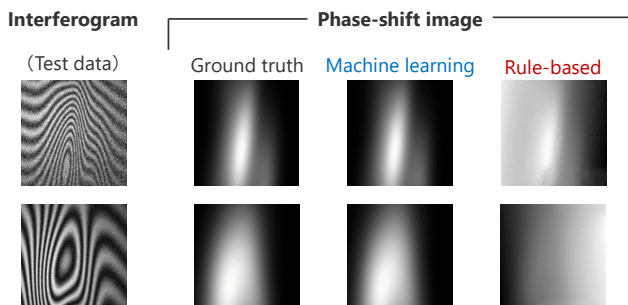


Figure 5. Examples of extraction results for the simulation data. The intensity ranges of each image are different, and the images are displayed so that the maximum value is white and the minimum value is black.

Results for experimental data

The figure 7 shows examples of the results of the phase extraction from the interferograms measured by actual experiment. From left to right, each image shows examples of the interferograms measured by actual experiment, the ground truths of phase-shift images (unknown), the results of the phase extraction using the trained network, and the results of the phase extraction using the rule-based algorithms.

The phase extraction from the interferograms measured by actual experiment using machine learning looks successful, and at least it looks better than using the rule-based algorithms. It means there is high possibility that the network trained by using the simulated interferograms and corresponding phase-shift images is available for the phase extraction from interferograms measured by actual experiment. However, we cannot determine the evaluation function because we don't know the ground truth of the phase-shift images in case of the interferogram measured by actual experiment.

The evaluation of validity of the extraction from interferograms measured by actual experiment is a future task.

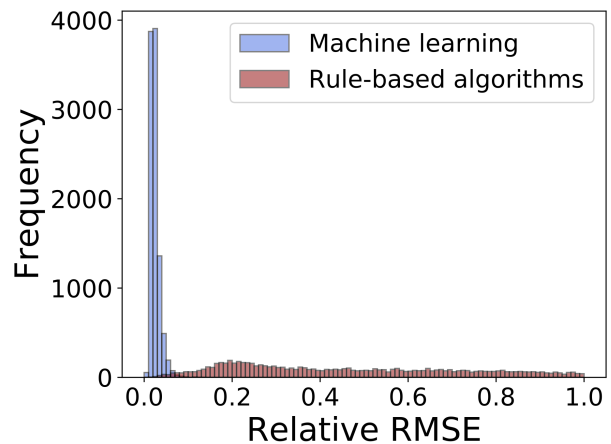


Figure 6. Histogram of E_2 by machine learning and rule-based algorithms for 10,000 test data. The data which have the relative root mean squared error of more than 1.0 are excluded.

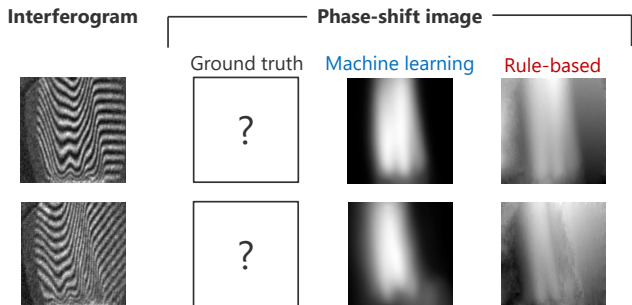


Figure 7. Examples of extraction results for the experimental data. The intensity ranges of each image are different, and the images are displayed so that the maximum value is white and the minimum value is black.

Conclusion

In this study, we focused on the ease of creating simulation data of interferograms and corresponding phase-shift images, and succeeded a new approach of phase extraction by machine learning using a large number of different patterns of simulation data. As the result, we realized drastic improvement in accuracy of phase-shift extraction and simplification of the process, which can contribute to the realization of three-dimensional refractive index distribution measurement of the object.

References

- [1] S. Tomioka, S. Nishiyama, S. Heshmat, Y. Hashimoto, and K. Kurita, Three-dimensional gas temperature measurements by computed tomography with incident angle variable interferometer, Proc. SPIE 9401, 94010J, 2015.
- [2] Ronneberger, O., Fischer, P., Brox, T.: U-net: Convolutional networks for biomedical image segmentation. In: MICCAI. LNCS, vol. 9351, pp. 234-241. Springer, 2015.
- [3] Kingma, Diederik P and Ba, Jimmy Lei. Adam: A method for stochastic optimization. arXiv preprint arXiv:1412.6980, 2014.
- [4] S. Tokui, K. Oono, S. Hido, and J. Clayton. Chainer: a next-generation open source framework for deep learning. In NIPS Workshop on Machine Learning Systems (LearningSys), 2015.

Author Biography

Daichi Kando received his degree of Master of Engineering in quantum science engineering from the Graduate School of Engineering, Hokkaido University, in 2017. Currently, he is a doctoral student in the Division of Quantum Science and Engineering, Graduate School of Engineering, Hokkaido University. His current research interests include interferometry data, image processing using deep learning.

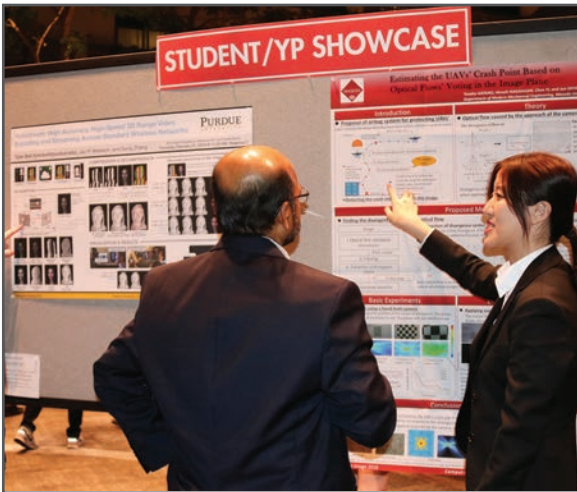
JOIN US AT THE NEXT EI!

IS&T International Symposium on

Electronic Imaging

SCIENCE AND TECHNOLOGY

Imaging across applications . . . Where industry and academia meet!



- **SHORT COURSES • EXHIBITS • DEMONSTRATION SESSION • PLENARY TALKS •**
- **INTERACTIVE PAPER SESSION • SPECIAL EVENTS • TECHNICAL SESSIONS •**

www.electronicimaging.org

